J. Electroanal. Chem., 339 (1992) 123–146
Elsevier Sequoia S.A., Lausanne
JEC 02184

Surface orientation dependence of oxide film growth at platinum single crystals *

Brian E. Conway and Gregory Jerkiewicz **
University of Ottawa, Department of Chemistry, Ottawa, Ontario K1N 6N5 (Canada)
(Received 26 February 1992; in revised form 29 April 1992)

Abstract

At single-crystal surfaces of noble metals, the initial sub-monolayer stages of anodic oxide film formation are distinguishable as two-dimensional surface processes specific to the geometry and orientation of the metal surface plane from which they originate. Below and beyond the monolayer level of oxide film formation, the extension of the film is logarithmic in polarization time for a given controlled electrode potential.

The purpose of the present paper is to investigate if and how the continuing logarithmic film growth process may also depend on single-crystal surface orientation, and thus be determined by the geometry of the metal surface underlying the growing oxide film.

The underpotential deposition hydrogen profiles, determined following the reduction of small and larger quantities per square centimetre of the oxide film at platinum, show that the geometry of the underlying platinum metal surface on which the oxide film was developed changes detectably with respect to that of the initial oxide-free surface but still retains, to a large extent, its initial two-dimensional structure. Once the Pt(111) or Pt(100) surfaces have been altered by the initial monolayer, they remain essentially unchanged during further oxide formation. The resulting structures are characteristically different from one another and from that of polycrystalline platinum, and remain so (as indicated by underpotential deposition hydrogen profiles following film reduction) even after development of oxide films equivalent to ca. 1000 μC cm^{-2} in formation charge. Thus, the apparent crystal-face dependence of the oxide film growth kinetics reflects a true specificity with respect to the surfaces from which the films respectively originate.

* This paper is presented in honour of Professor E.B. Yeager on the occasion of his retirement from the Department of Chemistry, Case Western Reserve University, Cleveland, OH, USA.
** Present address: Department of Chemistry, University of Sherbrooke, Sherbrooke, Quebec J1K 2R1, Canada.

INTRODUCTION

Knowledge of the state of anodically formed oxide films at platinum and other noble metals [1–13] is of major importance in electrode-kinetic studies of the O_2 and Cl_2 evolution reactions and hydrocarbon formation (the Kolbe reaction) as well as some ionic redox reactions [13], since it is the exterior surface of the platinum oxide film which determines the electrocatalytic properties of the electrode [10,11,12,14]. The state of the oxide film can be determined by cyclic voltammetry [9,10,11,15], optical [3,14,16] or X-ray photoelectron spectroscopy [17–20] measurements.

At the noble metals, the very earliest stages of oxide film formation at initially "bare", i.e. film-free, metal surfaces can be followed anodically as two-dimensional (2-d) surface processes [9,15,21,22]. Film growth is controllable in time and anodization potential [3,7,8,9,15] and one of the most significant results is that the transition from 2-d film formation to quasi-3-d, or 3-d bulk oxide film generation can be followed quantitatively [9,10,23]. Hitherto, such studies have been limited to polycrystalline platinum, gold and ruthenium surfaces [1–11,24,25] although regular cyclic voltammetry experiments at single-crystal platinum [26] and gold [15,27] surfaces have provided interesting information on the specificity of the initial stage of 2-d oxide-film formation processes, as a function of potential, with respect to crystal-face orientation and corresponding surface lattice structure. The film growth kinetics have not, however, been examined at single-crystal noble metal surfaces. In the present paper, we report such studies at Pt(111), Pt(100) and comparatively at polycrystalline platinum ["Pt(poly)"].

At submonolayer levels of coverage θ at platinum, rhodium, ruthenium and gold, the reversibility of formation and reduction of the oxygen-containing species in quasi-2-d films can be clearly distinguished voltammetrically [9,15,25,28] or optically [5,16] from that of thicker oxide films ("θ" > 1) which are irreversibly reducible owing to place-exchange [4,9,27,29,30].

The initial stages of oxide film formation at noble metals appear, at least qualitatively (cf. refs. 4, 9, 27, 30), to be well accounted for by the place-exchange mechanism [9], probably up to the now well characterized limit [24,31–33] of 2-d oxide film formation ("PtOPtO") [33] that is observable at platinum [4,9,27,30,34]. The formation of thicker films that can be observed at platinum [8,14,35–42] and also at ruthenium [28] or gold [43] probably proceeds by a mechanism of metal ion injection into and through the already formed inner (cf. refs. 44, 45) 2-d films, with a positive change of oxidation number of the metal ions [18–20] as they enter the growing thicker film on the outside of the underlying [44] quasi-2-d film.

Both these types of processes may depend on the 2-d coordination and lattice structure of the metal surface at which place-exchange takes place or from which metal ion injection into the growing film occurs.

Formation of thick oxide films at polycrystalline platinum electrodes (up to 50 equivalent monolayers of "PtO") has been studied extensively [32,35–42,46] and previous works [7,8,23,47] on Pt(poly) reveal that the growth of the oxide film is

logarithmic in polarization time at constant electrode potential, in the range of potentials where oxide-film formation takes place. It is interesting that at low extents of oxide film generation, the linear logarithmic relation passes through the limit for monolayer OH or oxygen coverage without change of slope. The possible origins of a direct logarithmic film growth law, in relation to the above independence of growth rate on attainment of monolayer OH or oxygen coverage, have been treated by Conway et al. [23] in terms of time-dependent surface dipole moment changes (due to deposition of OH and oxygen species in 2-d film formation) and by Gilroy [8] in terms of a "nucleation-and-growth" mechanism. Thicker film formation has been treated in terms of the Mott–Cabrera mechanism [3,5,6,48].

Some recent experiments have led us to the interesting observation (see Fig. 1) that the thickness of anodic platinum oxide films is different at the various observable grains exposed at the surface of a polycrystalline platinum electrode. Since grains within a polycrystalline platinum electrode are presumably single crystals (but possibly disordered or restructured), it is clear that the oxide growth rate probably depends on the crystallographic orientation of the metal and varies from one grain to another. While much attention has been devoted to the study of oxide films, both thin and thick, at polycrystalline platinum, we are unaware of any data on the oxide growth behaviour upon anodic polarization at single-crystal platinum electrode surfaces.

The purpose of the present paper is therefore to investigate if, and how, the kinetics of anodic oxide film growth at platinum depend on the surface orientation and 2-d lattice structure of the surface using two well defined single-crystal surfaces since the behaviour indicated in the micrograph in Fig. 1 only provides a qualitative distinction between extents of oxide film formation at various grains (of unknown orientations).

It should be mentioned that interpretation of the cyclic voltammetry current vs. potential profiles for single-crystal platinum electrodes, recorded by Hubbard et al. [26], Clavilier and coworkers [49–55] and other researchers [56–59] may provide indirectly some limited information on the oxide formation but not on the kinetics of its growth. For instance, existing reports on "quenched" Pt(111) indicate [49,51,55] that formation of the quasi-2-d oxide does not set in below a potential of 1.10 V, RHE, while on an electrochemically cleaned Pt(111) surface it starts at the same potential as for polycrystalline platinum, i.e. at ca. 0.85 V, RHE. In the case of Pt(100), the formation of the quasi-2-d oxide begins at ca. 0.80 V, RHE, while for Pt(111) it commences between 0.80 and 0.90 V, RHE, depending on the history of thermal treatment of the electrode [51,52,54,55].

Pre-electrochemical formation of oxide on single-crystal and polycrystalline platinum electrodes can also be observed [50–52] when electrodes are flame annealed followed by quenching in water. The existence of such an oxide film is indicated from the form of the first negative-going sweep taken from the rest potential of flame-annealed platinum electrodes, which is around ca. 0.90 V, RHE

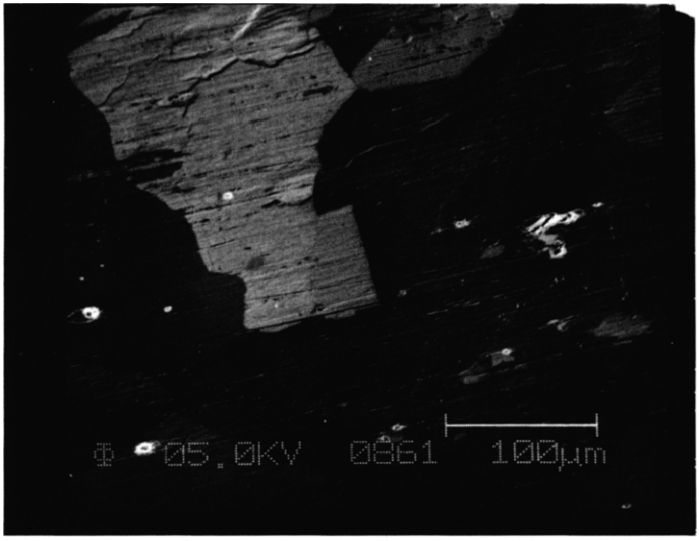

(a)

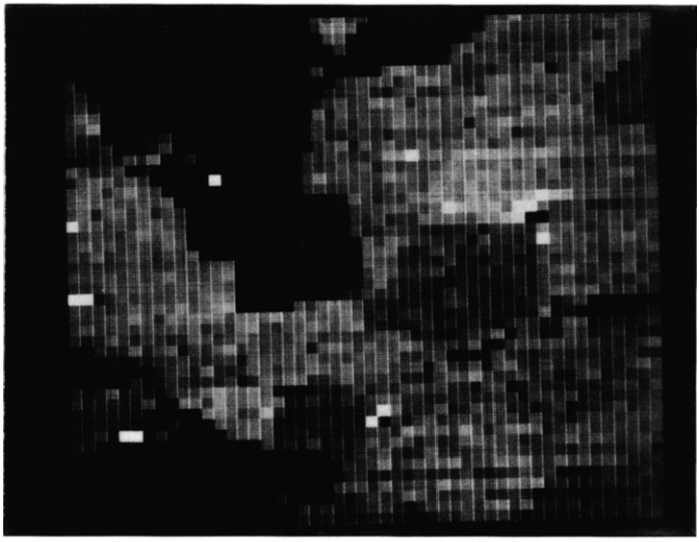

(b)

Fig. 1. SEM EDS mapping analysis micrographs: (a) showing different grains within a polycrystalline platinum sheet covered with platinum oxide; (b) EDS mapping analysis micrographs. The dark spots represent a higher platinum content while the bright spots represent higher oxygen content.

(compare with the rest potential of an oxide-free platinum electrode which is ca. 0.85 V).

EXPERIMENTAL

1. Electrode preparation

The Pt(111) and Pt(100) electrodes, supplied by Goodfellow, Cambridge, UK, had a cylindrical shape (3 mm in diameter, 10 mm in length) and were of 99.999% purity. The electrical contact was made by connecting the platinum single crystals to a 99.98% pure platinum wire by means of a tiny pre-formed gold (99.98%) bead which provided a stable, reliable and non-contaminating join, even when the platinum single crystals had to be re-annealed in high vacuum at 900°C. The procedure applied to mount, polish and clean platinum single crystals was as described elsewhere [57,60]. Clean polycrystalline platinum electrodes were prepared by a well known and established procedure [9].

2. Electrode orientation

The crystallographic orientations of the Pt(111) and Pt(100) crystals were determined using the back-reflection von Laue method described by Hamelin [61]. This procedure was repeated after mounting, polishing and annealing. Also, the characteristic channelling patterns [60,62] of the crystals were obtained (Fig. 2).

3. Solution and cell

High-purity 0.5 mol dm^{-3} solution was prepared by dilution of BDH Aristar grade H_2SO_4 in pyrolytically distilled water (PDW). In this solution, the electrolyte anion is principally HSO_4^-. A standard, three-compartment, Pyrex all-glass cell, with sleeved stopcocks, was employed as in previous work [9,38,63].

4. Instrumentation

Standard instrumentation was employed for recording linear-sweep voltammograms, as described elsewhere [9,57,60,63]. All potentials are quoted with respect to the hydrogen reference electrode in the same solution.

5. Surface area and charge evaluation

The single-crystal surfaces were polished to a mirror-like finish and the roughness factor R was assumed to be virtually equal to unity ($R = 1$), i.e. the real surface areas could be assumed to be equivalent to the geometric areas which were 0.0895 (± 0.005) cm^2 for Pt(111) and 0.0628 (± 0.005) cm^2 for Pt(100) [57,60]. The real surface area of the polycrystalline platinum electrode used was determined

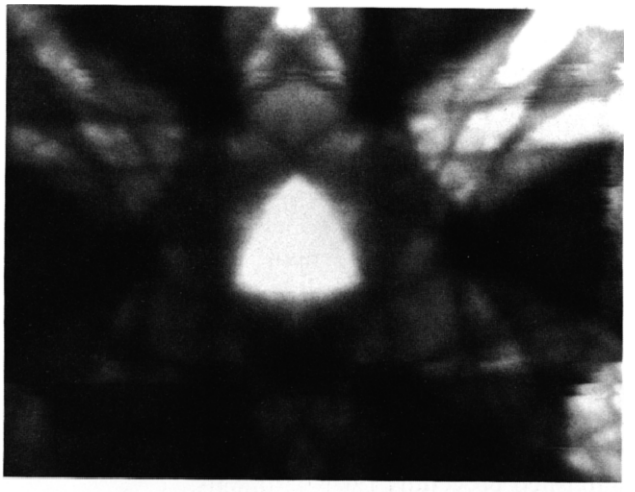

(a)

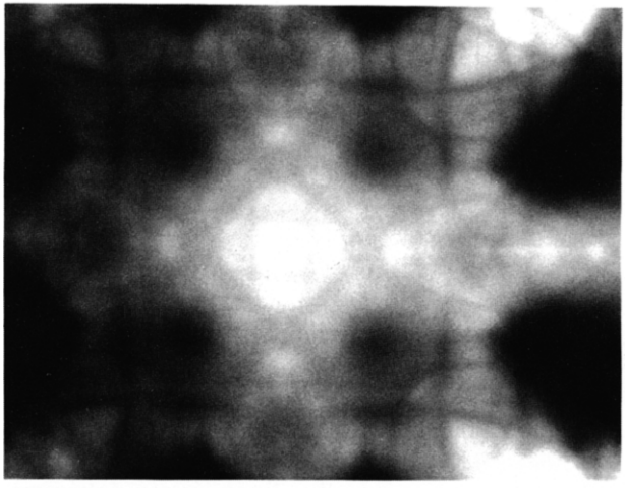

(b)

Fig. 2. Channelling patterns of platinum single crystals: (a) Pt(111), and (b) Pt(100).

from the hydrogen underpotential deposition (UPD) accommodation by taking 220 μC cm^{-2} as the charge density for monolayer hydrogen deposition [9,63].

Evaluation of charges Q_{ox} for the oxide films was made by integration of the i vs. E profiles, allowing for the double-layer charging contribution. The "theoretical" hydrogen UPD charges used for Pt(111) and Pt(100), Q_{HUPD}, were those adopted by Hubbard et al. [26], i.e. 240 and 208 μC cm^{-2} respectively.

RESULTS AND DISCUSSION

The cyclic voltammetry current vs. potential profiles for Pt(111) and Pt(100) recorded during the course of the present work were consistent with the results of other laboratories [49–58,60,64]. Here, we present the results of oxide growth on the (111) and (100) surfaces of platinum single-crystal electrodes in comparison with corresponding results for Pt(poly).

It is to be noted that growth of oxide examined in the present work refers to the increase in extent of formation of the quasi-2-d state which we have denoted as "OCl" and Shibata and Sumino [36] have designated as "α". This state corresponds to that identified (in reduction) by the single cathodic current peak in cyclic voltammetry experiments, as illustrated in Figs. 8(a), 9(a) and 9(b) later. The growth of this state of the surface oxide reaches, however, a limit corresponding nominally to "Pt–O–Pt–O" in the representation of Parsons and Visscher [33] from their ellipsometry experiments and to the corresponding limit noted by Biegler and Woods [24] based on cyclic voltammetry experiments.

This limit corresponds to a reduction charge of ca. 880 μC cm^{-2} after correction for the change in real area that arises on account of thicker oxide film formation, as determined by UPD hydrogen accommodation. However, the overall growth of the oxide film continues logarithmically in time (Fig. 4) owing to parallel increases of other states (cf. refs. 23, 32, 36, 46) of the oxide which arise as a result of polarization at potentials beyond 1.8 V, RHE for long times and are clearly distinguishable in linear sweep voltammetry experiments.

Extents of oxide film growth at Pt(111) and Pt(100) were determined as follows: (a) by application of a single sweep to a potential controlled between 0.90 and 1.80 V, RHE; (b) by potentiostatic polarization at potentials E_h held between 0.90 and 1.80 V, RHE, for various holding (polarization) times T_h which were 0, 10, 100 and 1000 s. As found in previous works, the extents of film growth are logarithmic in t_h, and were derived from the reduction current profiles for each of the E_h values by integration, in the usual way, allowing for a double-layer charging contribution. From these data, the logarithmic rates, d Q_{ox}/d log t_h, of oxide formation could be calculated. The smallest oxide coverage developed was obviously for $E_h = 0.90$ V, RHE, and $t_h = 0$ s.

1. Oxide formation in a single sweep to potentials between 0.90 and 1.80 V, RHE

Figure 3 shows the oxide-reduction charges for Pt(111), Pt(100) and Pt(poly) electrodes upon application of a single sweep as a function of the upper potential limit E_h at 298 K. Under these conditions, the state designated OCl [9], i.e. the quasi-2-d oxide, is observed in the usual way in the reduction peak following polarization at E_h. The "thickest" oxide film at Pt(111) was formed to an extent of 1.79 equivalent "PtO" nominal monolayers ($Q_{ox} = 865$ μC cm^{-2}) while that at Pt(100) was 2.67 "PtO" nominal monolayers ($Q_{ox} = 1100$ μC cm^{-2}).

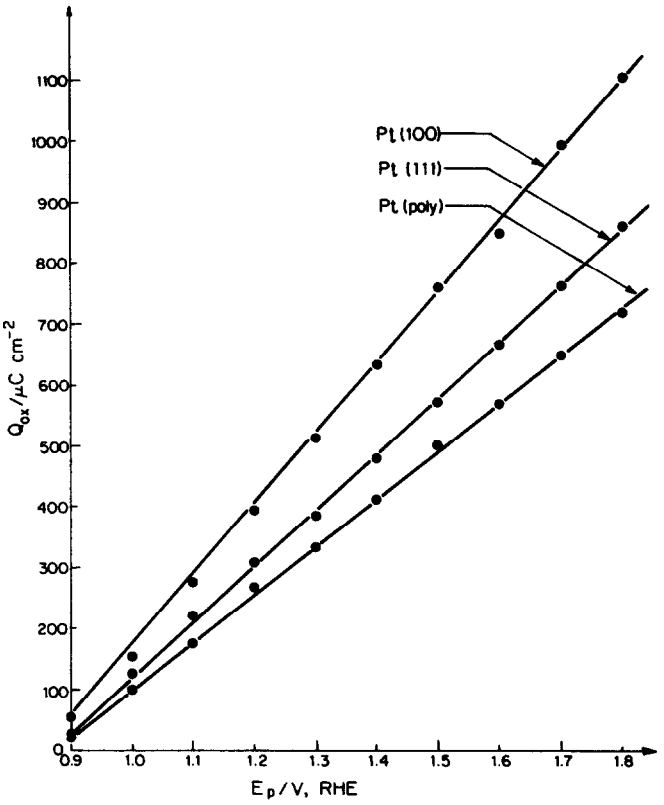

Fig. 3. Oxide-reduction charges for Pt(111), Pt(100) and Pt(poly) electrodes upon a single sweep as a function of the upper potential limit (0.5 M aq. H_2SO_4, 298 K).

The significant feature of the results presented in Fig. 3 is that the extent of oxide formation in a single sweep at Pt(100) is evidently substantially greater than that at Pt(111) or Pt(poly). This observation is discussed further later in this paper.

2. Oxide growth for various polarization potentials and times

Oxide film development was followed by maintaining the potential for various times t_h at polarization (holding) potentials E_h between 0.90 and 1.80 V, RHE. The resulting logarithmic oxide growth rates are shown in Figs. 4 and 5. The "thickness" of the oxide formed at Pt(111), for $E_h = 1.80$ V and $t_h = 1000$ s, was equivalent to a charge $Q_{ox} = 1300\ \mu C\ cm^{-2}$ (i.e. 2.71 equivalent "PtO" monolayers) while that at Pt(100) was $Q_{ox} = 1456\ \mu C\ cm^{-2}$ (3.50 equivalent "PtO" layers). Again, the oxide growth rate at Pt(100) was significantly greater than that at Pt(111). Analogous results for polycrystalline platinum are shown in Fig. 6. The

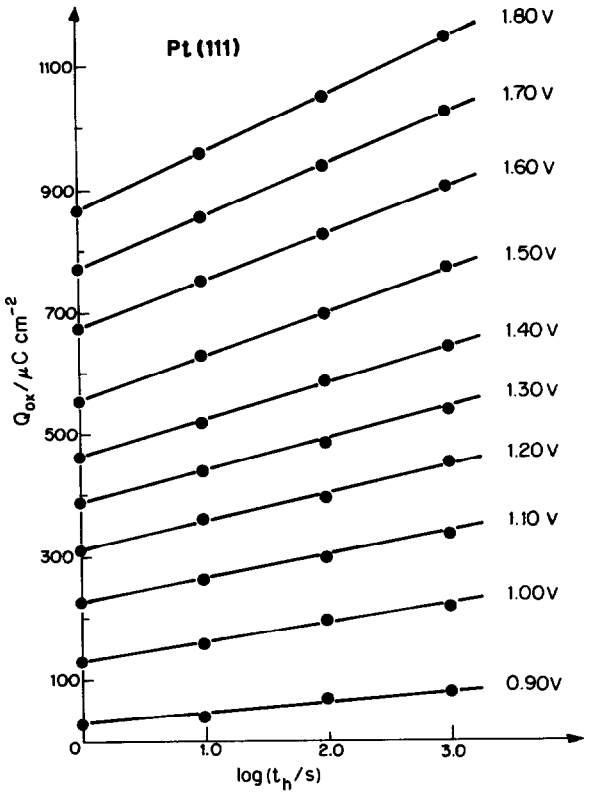

Fig. 4. Logarithmic oxide film growth plots, Q_{ox} vs. log t_h, at Pt(111) for various polarization potentials E_h (0.5 M aq. H_2SO_4, 298 K).

kinetics of the oxide growth will be discussed later; however, it should be mentioned that (a) the Q_{ox} vs. log t_h plots are linear, i.e. the oxide growth proceeds according to the direct logarithmic law observed [7,11] and discussed [8,23] previously, (b) the values of the slopes d Q_{ox}/d log t_h depend on E_h as shown in Fig. 7, and (c) the Q_{ox} vs. log t_h plots pass through the monolayer level of oxide coverage (expressed as charge) with no change of slope; this is an important feature, noted previously [11,23] for polycrystalline platinum.

3. Maintenance of surface geometry of the platinum during film growth

It is important first to establish whether or not the structures of the platinum single-crystal surfaces (which are well known to be characteristically indicated by their cyclic voltammetry profile "signatures" in the UPD hydrogen region) respectively remain essentially the same during the course of progressive increase of extent of oxide film formation.

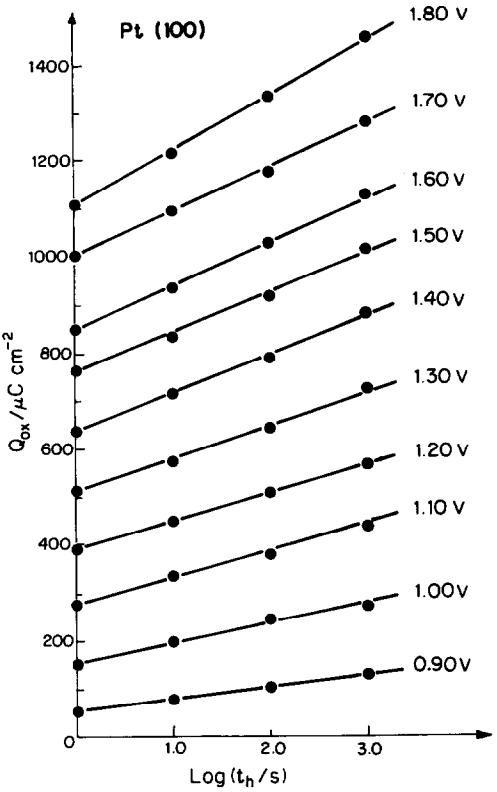

Fig. 5. Logarithmic oxide film growth plots, Q_{ox} vs. log t_h, at Pt(100) for various polarization potentials (0.5 M aq. H_2SO_4, 298 K).

A remark must first be made about the initial condition of the Pt(111) and (100) surfaces. The results presented in this paper were obtained on thermally annealed surfaces (not quenched as in the Clavilier technique). Under such experimental conditions, the hydrogen UPD profiles differ significantly from those of Clavilier et al. [49–55] but were closely similar to those of Hubbard et al. [26] for supposedly well characterized Pt(111) surfaces. However, Mooto and Furuya [65] found that heating a Pt(111) crystal surface in H_2 at 270°C maintained the Clavilier-type surface while heating in O_2 below 540°C led to the Hubbard type cyclic voltammetry profile. In a forthcoming paper, we shall show results obtained from comparative reflective high energy electron diffraction measurements on thermally annealed, fast cooled and quenched platinum single crystals having the (111) and (100) orientations.

Aberdam et al. [64] and the present authors [57] have demonstrated the transition of the "Clavilier-type" UPD hydrogen cyclic voltammogram to the "Hubbard-type" [26] upon potential cycling several times into the region of

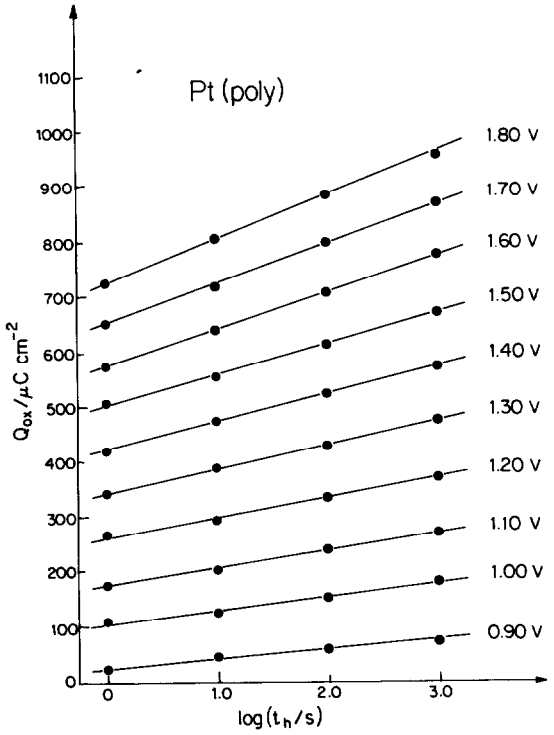

Fig. 6. Logarithmic oxide film growth plots, Q_{ox} vs. log t_h, at Pt(poly) for various polarization potentials (0.5 M aq. H_2SO_4, 298 K).

oxide-film formation; it was demonstrated [57,64] that the UPD hydrogen profile undergoes significant and irreversible changes upon such conditions of oxide film formation and reduction. Aberdam et al. [64] demonstrated by low energy electron diffraction (LEED) measurements that the Hubbard-type [26] UPD hydrogen profile represents a restructured surface having, however, still ca. 90% of the surface as (111) oriented terraces. This is probably the state of our nominal "(111) surfaces" after our thermal annealing treatment.

The origin of the substantial differences between the "Hubbard-type" and "Clavilier-type" UPD hydrogen profiles for Pt"(111)" surfaces remains the subject of current discussion; in another paper [57] we have suggested that the difference may arise because of some frozen disorder in the (111) surface introduced by the procedure of quenching a thermally excited surface very rapidly to room temperature in water, a process that also gives rise [54] to a thermochemically formed oxide film on the quenched surface. The introduction of a frozen state of disorder in the structure of the (111) surface by quenching in water from a temperature of about 1000–1100°C received strong support from the recent observations of Uchida and Lehmpfuhl [67] who found substantial surface imperfection densities in such

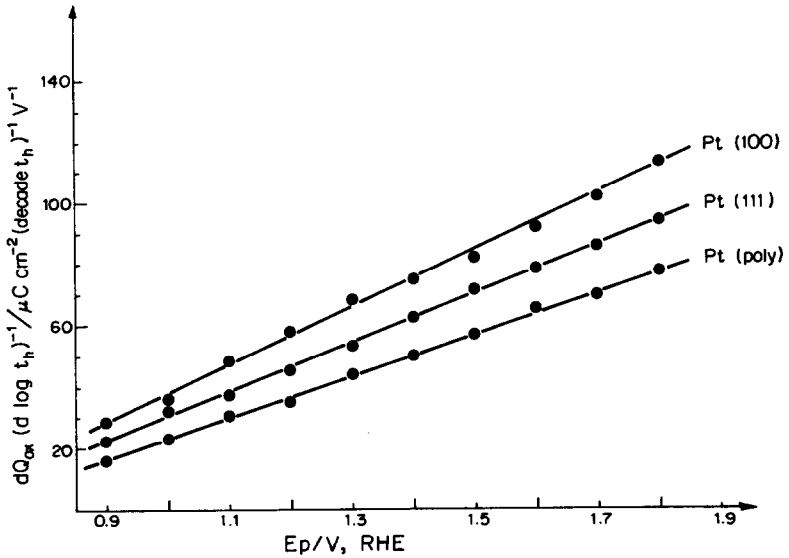

Fig. 7. Slopes of the Q_{ox} vs. log t_h plots as a function of the polarization (holding) potential E_h for Pt(111), Pt(100) and Pt(poly).

quenched surfaces. Such results raise the question, to which we directed attention [57], of whether in fact, the Clavilier-type (111) surface (formed by quenching from high temperatures) is at all a well ordered surface (on the atomic scale) of real (111) structure. The fact that LEED observations do indicate a (111) surface may only reflect the fact that such diffraction experiments only see long-range order.

A recent review [68] on thermal treatments of metal surfaces provides much evidence for introduction of a defect density distribution in the heat-treated surfaces; in fact, at a number of metals, a surface-roughening transition temperature arises associated with Boltzmannianly excited point defects.

It is well established [4,9,29] that the oxide film formation proceeds through the place-exchange mechanism during which the platinum atoms and ions at the surface exchange their places with oxygen-containing species; then it would follow that it is not only the geometry of the first layer of platinum atoms but also of those located at least one layer beneath that determine the kinetics of the oxide formation. Since the initial stage of oxide film formation causes restructuring, mostly of the first metal monolayer without affecting deeper levels, the structural changes of the first monolayer, though significant, may not be crucial for the further development of the oxide film.

Figure 8(a) shows the UPD hydrogen adsorption–desorption profiles and the oxide reduction profiles for the Pt(111) surface upon application of a single sweep to various upper potential limits between 0.9 and 1.8 V, RHE. Figure 8(b) shows the corresponding profile after five cycles up to 1.40 V, RHE: there are only small

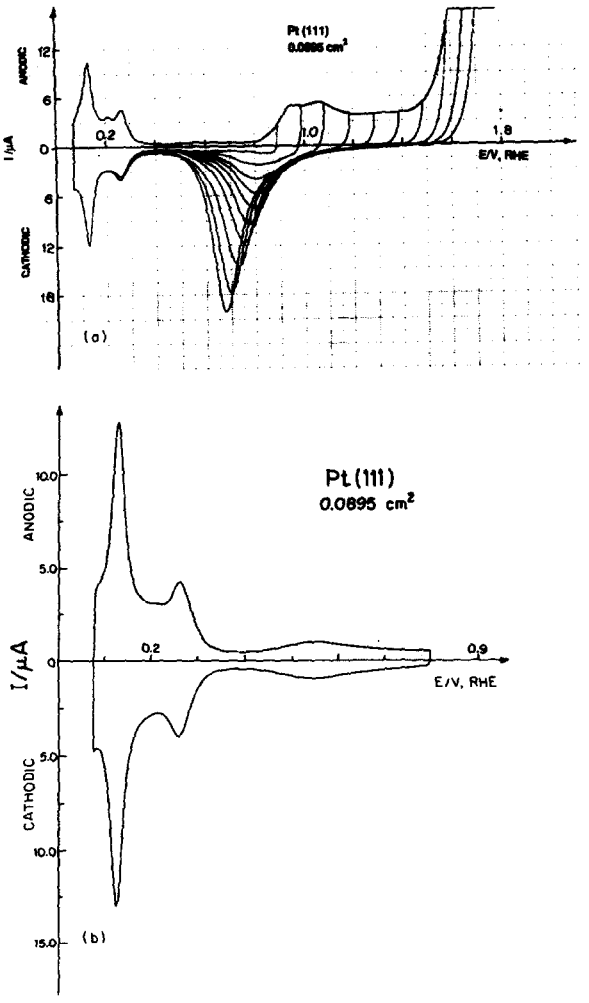

Fig. 8. (a) Cyclic voltammetry profiles for reduction of surface oxide grown on Pt(111) by application of a single sweep from 0.90 to 1.60 V, RHE (0.5 M aq. H_2SO_4, 298 K). (b) Cyclic voltammetry profile for Pt(111) after five cycles up to 1.40 V, RHE (0.5 M aq. H_2SO_4, 298 K).

differences discernable, so it may be concluded that the oxide film growth takes place at an underlying metal surface which, although significantly changed from the initial Clavilier-type surface (exhibiting the now well known "double butterfly" form of UPD profile in cyclic voltammetry), has an orientation and structure that is maintained with little change during the progressively increasing extent of formation of the oxide film. Only after formation of oxide films to much large thickness

(greater than about 10 equivalent "PtO" monolayers) does the UPD hydrogen profile change after film reduction owing to significant disordering of the surface region. The behaviour of the thin films confirms (cf. ref. 57) the greater surface-structural stability of the "Hubbard-type" of (111) surface over that of the initial "Clavilier-type" surface. This is consistent with our observation [57] that the former type of surface can result just from thermal annealing alone in a nominal vacuum (but not ultrahigh vacuum), so effects of traces of O_2 could be responsible for this transformation.

An interesting feature of the profiles shown in Figs. 8(a) and 8(b) is their similarity to the behaviour of a polycrystalline platinum surface; thus, in refs. 66, 69, 70 it was demonstrated that drawn platinum wires contain substantial grains or domains having principally a (111) orientation (but probably restructured or stepped).

Similar conclusions arise from the behaviour of the (100) surface but the changes in the UPD hydrogen profiles are less dramatic than in the case of the (111) surface. Figure 9(a) shows the UPD hydrogen adsorption–desorption profiles and the oxide reduction profiles for the Pt(100) surface upon application of a single sweep to various positive potential limits up to 1.8 V, RHE. Figure 9(b) shows the corresponding profile after five cycles up to 1.40 V, RHE. It is clear that the UPD hydrogen profiles, determined for the (111) and (100) surfaces, remain quite different from one another and this is also the case even after polarization at potentials as high as 1.80 V for 1000 s, for which oxide films of appreciable thicknesses are generated (see Section 2).

The only ambiguity in the conclusions from the UPD hydrogen profiles recorded after oxide film reduction at the three types of platinum surfaces is the question of whether the process of reduction of the respective oxide films itself leads to new types of UPD hydrogen profiles differing from those recordable at the initial, oxide-free platinum surfaces. In our experience this is not the case, so our conclusions regarding maintenance of characteristic underlying surface geometries, beneath the growing films at Pt(100), nominal Pt(111) and Pt(poly), remain unimpaired.

It may therefore be concluded from these results that under the experimental conditions described in this paper, the growth of the oxide films does not convert the underlying surfaces of Pt(111) or (100) to some common (disordered and polycrystalline) structure.

4. Discussion of the oxide growth behaviour

First an important point arises in attempts to compare quantitatively the kinetics of oxide growth at various low-index single-crystal faces of platinum; the comparison cannot be made directly since different faces contain different numbers of platinum atoms per square centimetre. For a qualitative and quantitative discussion, it is therefore essential to introduce a normalization factor based on the UPD hydrogen accommodation for each of the principal low-index faces so

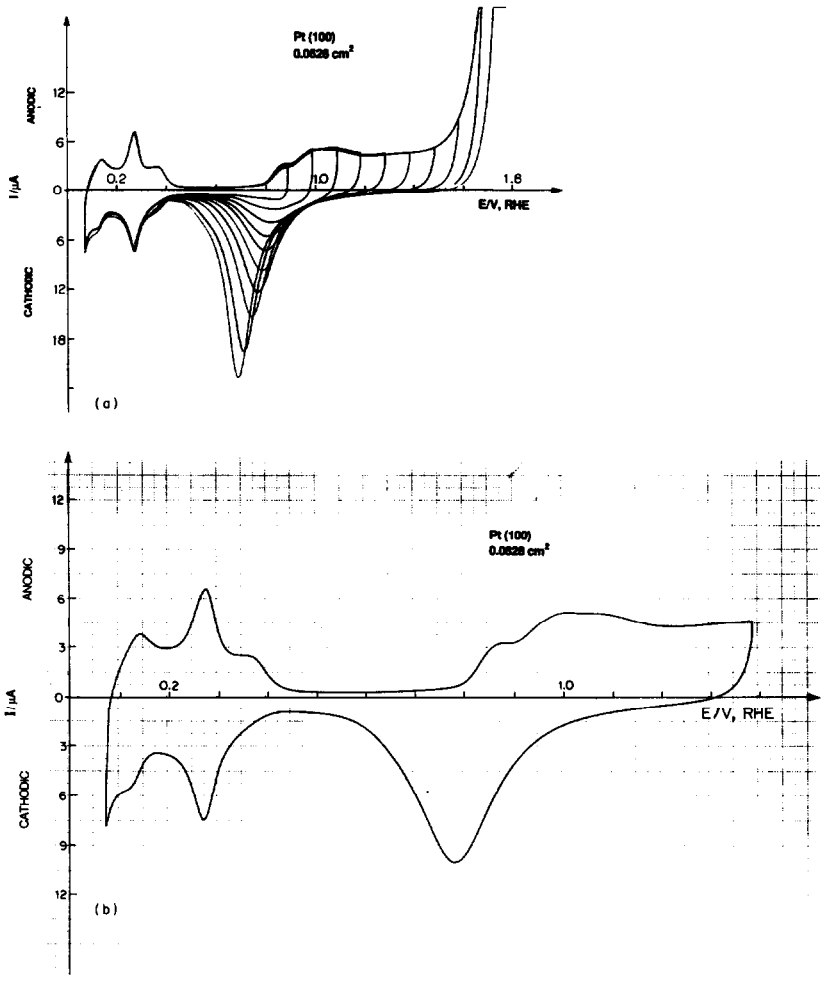

Fig. 9. (a) Cyclic voltammetry profiles for formation and reduction of surface oxide grown on Pt(100) by an application of a single sweep from 0.90 to 1.80 V, RHE (0.5 M aq. H_2SO_4, 298 K). (b) Cyclic voltammetry profile for Pt(100) after five cycles up to 1.40 V, RHE (0.5 M aq. H_2SO_4, 298 K).

that, after the normalization, the results for each face would refer to the same number of platinum atoms per actual square centimetre but in different coordination geometries. This requires definition of a "standard surface". The Pt(111), with its hydrogen UPD accommodation of 240 μC cm^{-2} [26], is taken here, arbitrarily, as the "standard surface" since it is the most stable out of the various single-crystal faces of the f.c.c. system [66]. The specific hydrogen UPD charge, divided by the electron charge e gives the "standard number" of platinum atoms per square centimetre in the Pt(111) electrode surface. Once having defined this standard

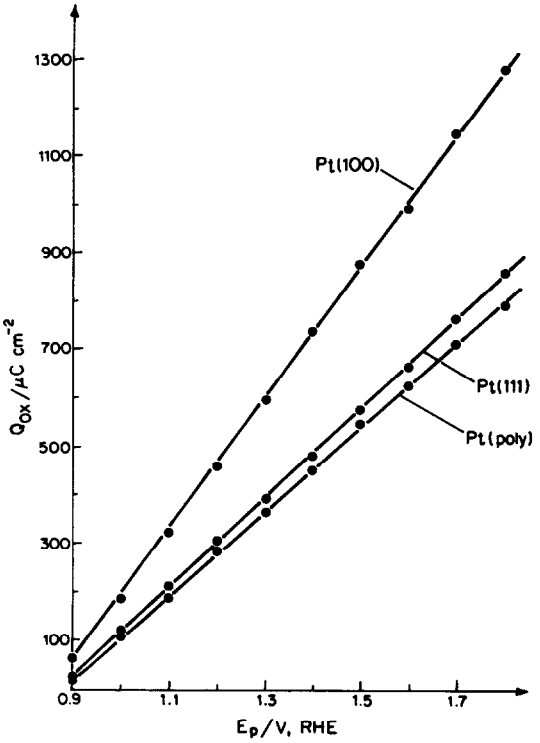

Fig. 10. Normalized oxide-reduction charges for Pt(111), Pt(100) and Pt(poly) electrodes upon a single sweep as a function of the upper potential limit (0.5 M aq. H_2SO_4, 298 K).

surface, the normalization factor would be evaluated according to the following formula:

$$n_f = \frac{\text{number of atoms per 1 cm}^2 \text{ of Pt(111) surface}}{\text{number of atoms per 1 cm}^2 \text{ of the investigated Pt surface}}$$

The values of the normalization factors for the low-index platinum faces and for Pt(poly) are then as follows:

$n_f(111) = 1.000$

$n_f(110) = 1.632$

$n_f(100) = 1.155$

$n_f(\text{poly}) = 1.092$

The normalized values of such experimentally determined oxide reduction charges are then derived by multiplying them by the appropriate normalization factor listed above. (The surface structure of polycrystalline platinum electrodes is not uniquely

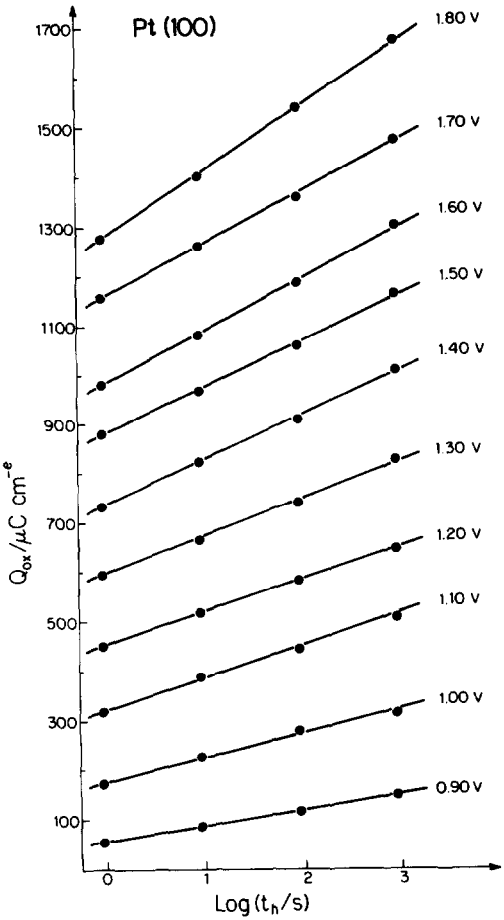

Fig. 11. Normalized logarithmic oxide film growth plots, Q_{ox} vs. log t_h, at Pt(100) for various polarization potentials (0.5 M aq. H_2SO_4, 298 K).

well defined (cf. Fig. 1). However, it is commonly found that drawn wires and rolled plates of platinum give a very reproducible form of the cyclic voltammetry current vs. potential profile for UPD of hydrogen, similar to that for platinized platinum.)

Figure 10 shows how the normalized oxide-reduction charges for oxide films grown at Pt(111), Pt(100) and Pt(poly) by application of a single sweep up to 1.80 V, RHE, depend on the growth potential E_h. Figures 11 and 12 show the normalized logarithmic oxide growth rates for Pt(100) and Pt(poly) for various holding (polarization) potentials E_h and times t_h. The plots for Pt(111) are, of course, unchanged since $n_f(111) = 1.000$ by convention here. The values of the

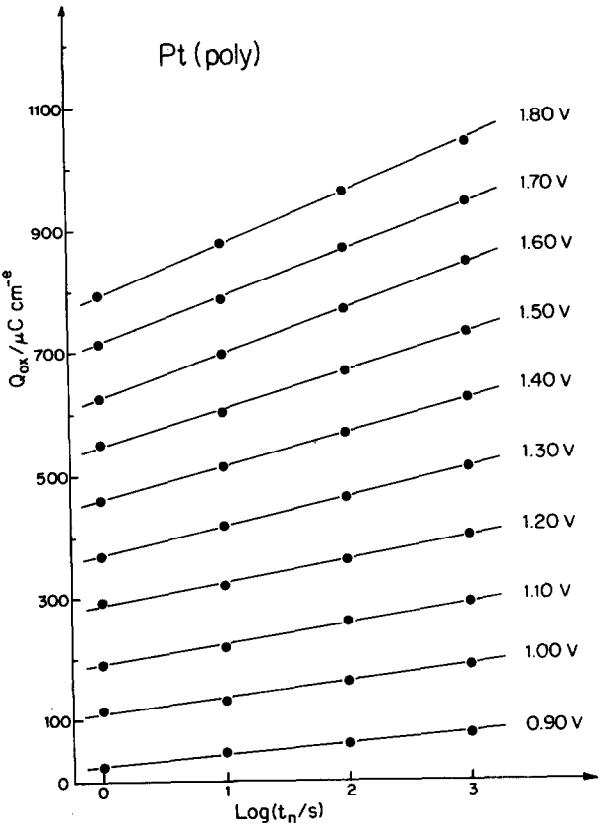

Fig. 12. Normalized logarithmic oxide film growth plots, Q_{ox} vs. log t_h, at Pt(poly) for various polarization potentials (0.5 M aq. H_2SO_4, 298 K).

slopes of these plots are shown in Fig. 13. These results clearly show that the oxide growth at Pt(100) is appreciably faster than that at Pt(111).

This behaviour could be rationalized as follows, recognizing that the oxide growth is commonly believed to proceed through a place-exchange mechanism [9,27]. Thus, in the case of the (111) surface, each platinum atom is coordinated by nine atoms (six lying in the same plane and three in the plane underneath) while, for (100), only eight atoms (four lying in the same plane and four underneath) coordinate a given surface atom. The situation would be more complex for reconstructed surfaces where there might be two or more kinds of surface atoms, each having its own characteristic surface coordination number. The assumption that all low-index surfaces have the ideal (1×1) structure, though a simplification, is satisfactory enough at this level of the discussion.

Thus, the geometry of the (111) face suggests that the platinum surface atoms would be held more strongly (by nine atoms) than those of the (100) face (by eight

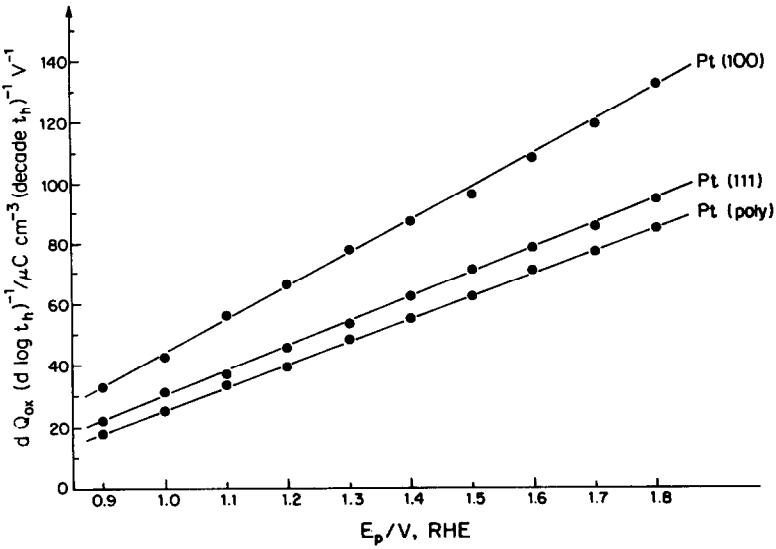

Fig. 13. Normalized slopes of the plots Q_{ox} vs. log t_h as a function of the polarization (holding) potential E_h for the Pt(100) and Pt(poly) surfaces. The slopes for Pt(111) are not changed upon normalization, as this is the "reference" surface.

atoms). Hence it is reasonable to expect that the rate of the place-exchange of platinum atoms with neighbouring oxygen-containing species would tend to be less at the (111) face than at the (100) face. The oxide-reduction charge for Pt(poly) falls close to that for Pt(111), indicating that the polycrystalline platinum surface contains a substantial fraction of crystallites having exposures of (111) orientation (most likely reconstructed, restructured or disordered) as has been concluded in various earlier works [66,69,70].

The Q_{ox} vs. log t_h plots (Figs. 4–6), extrapolated to the zero value of charge Q do not give a "common intercept" (i.e. when the oxide reduction charges are extrapolated to the zero value, the linear Q_{ox} vs. log t_h plots do not have the same intercept value, log $t \approx -12$), as had been reported in ref. 8 for polycrystalline platinum at various polarization potentials. On the contrary, the intercepts, designated log t_0, are seen to be significantly dependent on the E_h potential and their values are shown in Fig. 14. For the potential range from 0.90 to 1.80 V, RHE, the values of log t_0 in fact vary enormously, from about -1 to -10, but lie on a fairly common line for each of the three faces. It is informative to attempt to give to "log t_0" some physicochemical meaning. Roscoe and Conway [11] suggested that t_0 represents the small but finite time required for the potential to become adjusted across the electrode–solution interphase.

The observation that the Q_{ox} vs. log t_h plots do not have the same common intercept seems to be of importance for proper understanding of the oxide growth mechanism. The "nucleation-and-growth" mechanism of Gilroy [8] for platinum

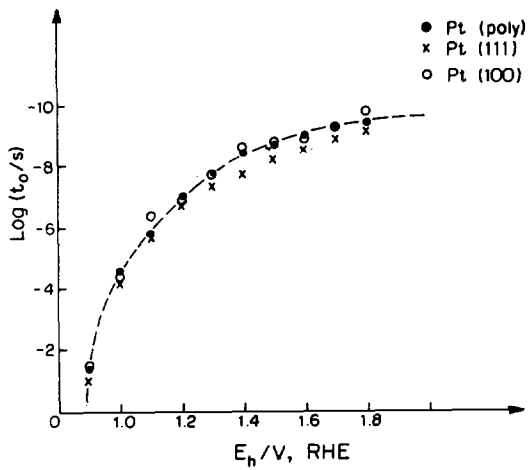

Fig. 14. The log t_0 vs. E_h relations for oxide growth kinetics at Pt(111), Pt(100) and Pt(poly) electrodes in 0.5 M H_2SO_4 at 298 K.

oxide growth was based on an observation that the intercepts of the Q_{ox} vs log t_h plots were common so that the relation $Q_{ox} = B \log (t/t_0)$ was the basis of the first step in his derivation of a kinetic equation for the oxide formation rate, based on nucleation-and-growth. An alternative approach to that of Gilroy was given by Conway et al. [23] who suggested that the experimentally observed features of the initial stages of formation of the quasi-2-d oxide film reveal rather an "under-potential-deposition" kind of behaviour than a "nucleation-and-growth" type. The observation that Q_{ox} vs. log t_h plots do not have a common intercept impairs the applicability of the growth mechanism model of Gilroy [8] for oxide formation in its initial stages.

The fact that oxide growth rates clearly depend on the orientation of the platinum surface at which the oxide grows, calls for further comment. It is unlikely that the growing oxide film can maintain any epitaxial relation to the surface of the underlying metal from which it develops since the structures and molar volumes of "PtO" or "PtO_2" states, which are probably hydrous in nature [41], must be very different from that of platinum in the crystalline metal. Therefore, the specificity of oxide growth kinetics to the surface from which the film develops must originate, we suggest, from the different rates at which continuing place-exchange occurs at the inner interface of the 2-d oxide film with the metal. This would be expected to be dependent on the geometry and coordination of that particular oriented surface, i.e. the interatomic binding energies of platinum atoms in these surfaces. Alternatively, the rate of platinum ion injection into the growing film (under "Mott–Cabrera" mechanism [3,48] conditions) would also probably be dependent on the orientation and coordination of the metal surface from which

such platinum ions originate. Note, however, that the Mott–Cabrera mechanism does not lead to a direct logarithmic law of oxide film growth in time.

In a recent discussion of the origin of the direct logarithmic growth law for oxide film development, Conway et al. [23] gave a mathematical treatment based on time-dependent change of the surface-dipole at noble metal interfaces due to extension of the oxide film in its quasi-2-d stage. Applied to single-crystal surfaces, this theory gives a qualitative basis for the surface orientation dependence of the logarithmic growth rate, $dQ/d \log t$, since the developing surface dipole potential, which modifies the local interfacial field, would be expected to be dependent on the geometry and electronic properties of each type of crystal surface plane. The above slope, according to eqn. (21) of ref. 23, is determined by the ratio of the dipole layer thickness d to the square of the surface dipole moment μ.

Finally, these results on the specificity of oxide film growth kinetics at single-crystal surfaces imply that virtually the same orientation of the given underlying surface is maintained during the process of progressive extension of the oxide film to appreciable but not large thicknesses, as is indicated by the surface-specific UPD hydrogen profiles that are maintained following oxide film reduction (Figs. 8 and 9).

CONCLUSIONS

The first studies on oxide film formation on platinum single-crystals by application of a single sweep and under potentiostatic polarization are reported. At the preliminary level to which the present work has been conducted, the principal conclusions are as follows.

(1) Formation of the quasi-2-d state of the oxide film at Pt(100) proceeds faster than at Pt(111), and that at Pt(111) is faster than at Pt(poly).
(2) Quantitative comparison of oxide growth rates at various low-index single-crystal faces of platinum and polycrystalline platinum requires introduction of a normalization factor so that, after such normalization, the results for various surfaces refer to the same number of platinum atoms per real square centimetre but in different surface coordination geometries.
(3) Normalization of the data for oxide growth rates at Pt(111), Pt(100) and Pt(poly) indicates that the oxide formation at Pt(100) is appreciably faster than at Pt(111) or Pt(poly).
(4) The rate of oxide formation at Pt(poly) falls close to that at Pt(111), suggesting that the polycrystalline platinum surface consists of crystallites or domains having mainly the (111) orientation, but probably restructured (stepped).
(5) Conclusion (3) can be rationalized if the oxide film growth proceeds by the place-exchange mechanism, i.e. if the place exchange rate is smaller on a high coordination surface Pt(111) than on a lower surface Pt(100) owing to different interatomic bonding energies.
(6) Differences of the oxide-growth rates at various single-crystal faces and polycrystalline platinum can be attributed to the different 2-d geometries of the

inner metal–metal-oxide interfaces (and corresponding 2-d coordinations of surface atoms). At which the place-exchange or platinum ion injection processes take place.

(7) The Q_{ox} vs. log t_h plots for Pt(111), Pt(100) or Pt(poly), at various potentials, do not have a "common intercept". This observation impairs the applicability of the "nucleation-and-growth" mechanism for the initial stages of oxide film growth at platinum.

ACKNOWLEDGMENT

Grateful acknowledgement is made to the Natural Sciences and Engineering Research Council of Canada for support of this work. G. Jerkiewicz gratefully acknowledges a Noranda/Bradfield Fellowship during the tenure of which this and other work was carried out at the University of Ottawa. We also thank Dr. H. Angerstein-Kozlowska, of this laboratory, for helpful suggestions and discussion.

REFERENCES

1 H.A. Laitinen and C.G. Enke, J. Electrochem. Soc., 107 (1960) 773.
2 K. Vetter and J.W. Schultze, J. Electroanal. Chem., 34 (1972) 131; 141.
3 J.L. Ord and F.C. Ho, J. Electrochem. Soc., 118 (1971) 46.
4 A.K.N. Reddy, M. Genshaw and J.O'M Bockris, J. Chem. Phys., 48 (1968) 671.
5 A. Damjanović and A.T. Ward, J. Electrochem. Soc., 121 (1974) 113 C; 126 (1973) 593d; 126 (1979) 555.
6 A. Damjanović and V.I. Birss, J. Electrochem. Soc., 130 (1983) 1688.
7 D. Gilroy and B.E. Conway, Can. J. Chem., 46 (1968) 875.
8 D. Gilroy, J. Electroanal. Chem., 71 (1976) 257; see also J. Electroanal. Chem., 83 (1977) 329.
9 H. Angerstein-Kozlowska, B.E. Conway and W.B.A. Sharp, J. Electroanal. Chem., 43 (1973) 9.
10 B.E. Conway and T.C. Liu, Langmuir, 6 (1990) 268.
11 S.G. Roscoe and B.E. Conway, J. Electroanal. Chem., 224 (1987) 163.
12 A.K. Vijh and B.E. Conway, Chem. Rev., 67 (1967) 623.
13 F.C. Anson, J. Am. Chem. Soc., 81 (1959) 1554; Anal. Chem., 33 (1961) 934.
14 S. Gottesfeld, M. Yaniv, D. Laser and S. Srinivasan, J. Phys., Coll. C5, suppl. 11, 38 (1977) 145; see also S. Gottesfeld, in A.J. Bard (ed.), Electroanalytical Chemistry, Vol. 15A, Marcel Dekker, New York, 1989.
15 H. Angerstein-Kozlowska, B.E. Conway, A. Hamelin and L. Stoicoviciu, J. Electroanal. Chem., 228 (1987) 429; see also Electrochim. Acta, 31 (1986) 1051.
16 S. Gottesfeld and B.E. Conway, J. Chem. Soc., Faraday Trans. I, 69 (1973) 1090.
17 J.S. Hammond and N. Winograd, J. Electroanal. Chem., 78 (1977) 55.
18 K.S. Kim, N. Winograd and R.E. Davis, J. Am. Chem. Soc., 93 (1971) 6296.
19 M. Peuckert, Electrochim. Acta, 29 (1984) 1315.
20 G.C. Allen, P.M. Tucker, A. Capon and R. Parsons, J. Electroanal. Chem., 50 (1974) 335.
21 F.G. Will and C.A. Knorr, Z. Elektrochem., 64 (1960) 2258.
22 D. Armstrong, M. Himsworth and J.A.V. Butler, Proc. R. Soc. London, Ser. A137 (1932) 604.
23 B.E. Conway, B.V. Tilak, B. Barnett and H. Angerstein-Kozlowska, J. Chem. Phys., 93 (1990) 8361.
24 T. Biegler and R. Woods, J. Electroanal. Chem., 20 (1969) 73; see also T. Biegler, D.A.J. Rand and R. Woods, J. Electroanal. Chem., 29 (1971) 269.
25 H. Angerstein-Kozlowska, B.E. Conway, A. Hamelin and L. Stoicioviciu, Electrochim. Acta, 31 (1986) 1051.

26 A.T. Hubbard, R.M. Ishikawa and J. Katekaru, J. Electroanal. Chem., 86 (1968) 271.
27 H. Angerstein-Kozlowska, B.E. Conway, B. Barnett and J. Mozota, J. Electroanal. Chem., 100 (1979) 417.
28 S. Hadži-Jordanov, B.E. Conway, H. Angerstein-Kozlowska and M. Vuković, J. Electrochem. Soc., 60 (1975) 359; see also J. Electrochem. Soc., 125 (1978) 1477.
29 N. Sato and M. Cohen, J. Electrochem. Soc., 111 (1964) 512.
30 B.V. Tilak, H. Angerstein-Kozlowska and B.E. Conway, J. Electroanal. Chem., 48 (1973) 1.
31 D.A.J. Rand and R. Woods, J. Electroanal. Chem., 35 (1972) 209.
32 G. Tremiliosi-Filho, G. Jerkiewicz and B.E. Conway, Langmuir, 8 (1992) 658.
33 R. Parsons and W.H.M. Visscher, J. Electroanal. Chem., 36 (1972) 329.
34 A.J. Appleby, J. Electrochem. Soc., 120 (1973) 1205.
35 S. Shibata, J. Electroanal. Chem., 89 (1978) 37.
36 S. Shibata and M. Sumino, Electrochim. Acta, 20 (1975) 739.
37 S.D. James, J. Electrochem. Soc., 116 (1969) 1681.
38 J. Balej and O. Spalek, Coll. Czech. Chem. Commun., 37 (1972) 499.
39 Y.B. Vassilyev, V.S. Bagotzky and O.A. Khazova, J. Electroanal. Chem., 181 (1984) 219; see also Y.B. Vassilyev, V.S. Bagotzky and V.A. Gromyko, J. Electroanal. Chem., 178 (1984) 247.
40 S. Shibata, Electrochim. Acta, 22 (1977) 175.
41 L.D. Burke and M.B.C. Roche, J. Electroanal. Chem., 137 (1982) 175.
42 L.D. Burke, in R.E. White, J.O'M Bockris and B.E. Conway (Eds.), Modern Aspects of Electrochemistry, Vol. 18, Plenum, New York, 1986, Chapter 4.
43 S. Barnartt, J. Electrochem. Soc., 106 (1959) 991.
44 B.E. Conway, G. Tremiliosi-Filho and G. Jerkiewicz, J. Electroanal. Chem., 297 (1991) 435.
45 M. Farebrother, M. Goledzinowski, G. Thomas and V.I. Birss, 297 (1991) 469.
46 T.C. Liu and B.E. Conway, Proc. R. Soc. London, Ser. A, 429 (1990) 375.
47 H. Angerstein-Kozlowska, B.E. Conway, K. Tellefsen and B. Barnett, Electrochim. Acta, 34 (1989) 1045.
48 N. Cabrera and N.F. Mott, Rep. Prog. Phys., 12 (1949) 163.
49 J. Clavilier, R. Fauré, G. Guinet and R. Durand, J. Electroanal. Chem., 107 (1980) 205; see also J. Clavilier, J. Electroanal. Chem., 107 (1980) 211.
50 J. Clavilier, D. Armand and B.L. Wu, J. Electroanal. Chem., 135 (1982) 159.
51 J. Clavilier and D. Armand, J. Electroanal. Chem., 199 (1986) 187.
52 J. Clavilier, R. Durand, G. Guinet and R. Faure, J. Electroanal. Chem., 127 (1981) 281.
53 J. Clavilier, D. Armand, S.G. Sun and M. Petit, J. Electroanal. Chem., 205 (1986) 267.
54 D. Armand and J. Clavilier, J. Electroanal. Chem., 263 (1989) 109.
55 J. Clavilier, K. El Achi, M. Petit, A. Rodes and M.A. Zamakchari, J. Electroanal. Chem., 295 (1990) 333.
56 P.N. Ross and F.T. Wagner, in H. Gerischer (Ed.), Advances in Electrochemistry and Electrochemical Engineering, Vol. 13, Interscience, New York, 1984; see also F.T. Wagner and P.N. Ross, J. Electroanal. Chem., 150 (1983) 141.
57 G. Jerkiewicz and B.E. Conway, J. Chim. Phys., 88 (1991) 1381.
58 A. Wieckowski, B.S. Schardt, S.D. Rosasco, J.L. Stickney and A.T. Hubbard, Surf. Sci., 146 (1984) 115.
59 A. Wieckowski, S.D. Rosasco, B.C. Schardt, J.L. Stickney and A.T. Hubbard, Inorg. Chem., 23 (1984) 565.
60 G. Jerkiewicz, Ph.D. Thesis, Chemistry, University of Ottawa, 1991.
61 A. Hamelin, in B.E. Conway, R.E. White and J.O'M. Bockris (Eds.), Modern Aspects of Electrochemistry, Vol. 16, B.E. Conway, Plenum, New York, 1985, Chapter 1.
62 I.M. Watt, The Principles and Practice of Electron Microscopy, Cambridge University Press, Cambridge, 1985.
63 B.E. Conway, W.B.A. Sharp, H. Angerstein-Kozlowska and E.E. Criddle, Anal. Chem., 45 (1973) 1321.

64 D. Aberdam, R. Durand, R. Fauré and F. El-Omar, Surf. Sci., 171 (1986) 303.
65 S. Mooto and N. Furuya, J. Electroanal. Chem., 172 (1984) 339.
66 G.A. Somorjai, Chemistry in Two Dimensions: Surfaces, Cornell University Press, Ithaca, NY, 1981.
67 Y. Uchida and G. Lehmpfuhl, Surf. Sci., 243 (1991) 193.
68 E.H. Conrad, Prog. Surf. Sci., 39 (1992) 65.
69 M.W. Roberts and C.S. McKee, Chemistry of the Metal–Gas Interface, Oxford University Press, Oxford, 1978.
70 Encyclopaedia of Physics (Polish edition), PWN, Warsaw, 1984.